TTK4190 Guidance and Control of Vehicles

Assignment 2

Written Fall 2019 By Kevin, Kevin, Dinosshan and Simen

Problem 1 - Open-loop analysis

Problem a

It is stated in the task that the wind velocity is zero, $V_w = 0$. This leads to the fact that the air velocity and the ground velocity is equal, $V_a = V_g$. This can be seen in fig. 1 where the vector V_w becomes the zero vector. The ground speed is therefore equal to the airspeed, which was given in the task.

$$V_g = V_a = 580km/h = 161.1m/s \tag{1}$$

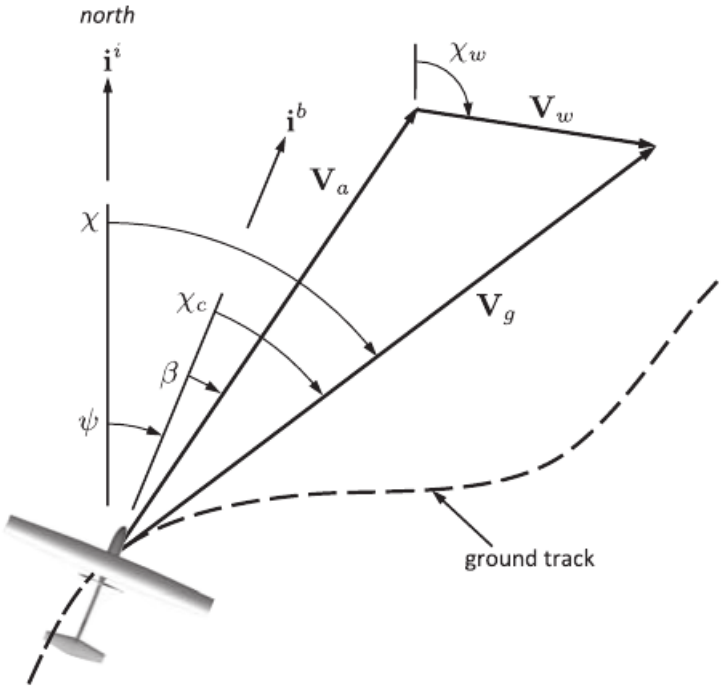

Figure 1: This figure shows the relationships between the wind-, ground- and air velocity vectors.

Problem b

The side-slip angle β can be expressed either as the relationship between the course angle χ, heading angle ψ, and the side-slip angle β, or as the relation between the components of the air velocity vector V_a expressed in body frame F^b. With the first method we get the relationship in eq. (2).

$$\begin{aligned} \chi &= \beta + \psi \\ \beta &= \chi - \psi \end{aligned} \tag{2}$$

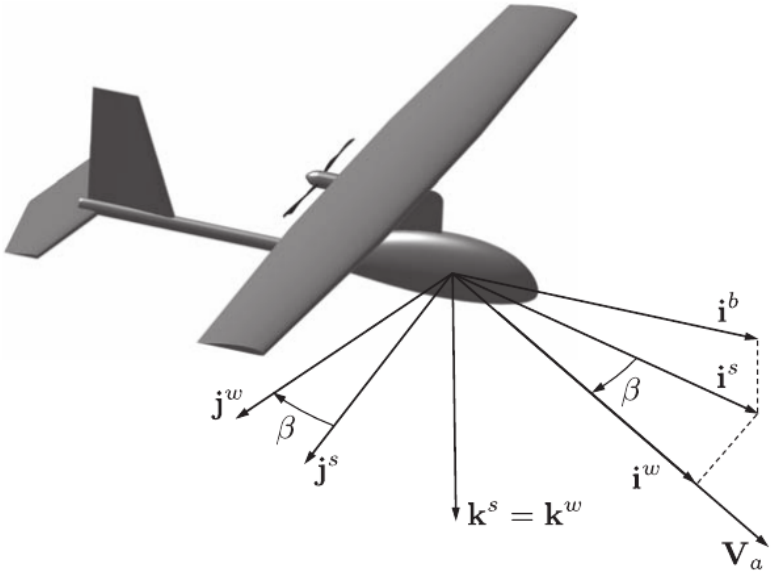

Figure 2: Here the connection between the wind frame and the stability frame can be seen. It is defined as an right hand rotation about k^s by β°.

With the second method we express β as the inverse sine of the ratio between the j^b component and the absolute value of the air velocity vector V_a^b.

$$V_a^b = \begin{pmatrix} u_r \\ v_r \\ w_r \end{pmatrix} = \begin{pmatrix} u - u_w \\ v - v_w \\ w - w_w \end{pmatrix} = V_g^b - V_w^b \tag{3}$$

$$\begin{aligned} \sin\beta = \frac{v_r}{|V_a|} &= \frac{v_r}{\sqrt{u_r^2 + v_r^2 + w_r^2}} \\ \Downarrow & \\ \beta = \arcsin\left(\frac{v_r}{\sqrt{u_r^2 + v_r^2 + w_r^2}}\right) & \end{aligned} \tag{4}$$

Problem c

In the duch-roll mode we focus on the sideslip and yaw states and neglect the effect of roll and aileron input. Since our model don't have rudder input the model for this mode is without input, as eq. (5) shows. The eigenvalues for this model is given by eq. (6).

$$\begin{pmatrix} \dot{\overline{\beta}} \\ \dot{\overline{r}} \end{pmatrix} = \begin{pmatrix} Y_v & \frac{Y_r}{V_a^* \cos\beta^*} \\ N_v V_a^* \cos\beta^* & N_r \end{pmatrix} \begin{pmatrix} \overline{\beta} \\ \overline{r} \end{pmatrix} \tag{5}$$

$$\lambda_{dutchroll} = \frac{Y_v + N_r}{2} \pm \sqrt{\left(\frac{Y_v + N_r}{2}\right)^2 - (Y_v N_r - N_v Y_r)} \tag{6}$$

We here find the values in our A matrix that correspond to the values in the A matrix for the dutch-roll mode.

$$\begin{aligned} Y_v &= -0.322 \\ N_r &= -0.32 \\ Y_v N_r &= -0.332 * -0.32 = 0.106 \\ N_v Y_r &= (N_v V_a^* \cos\beta^* *) \left(\frac{Y_r}{V_a^* \cos\beta^*} \right) = 6.87 * -1.12 = -7.69 \end{aligned} \tag{7}$$

$$\lambda_{dutchroll} = -\sigma \pm \omega_d = -0.32 \pm 2.8j \tag{8}$$

$$\begin{aligned} \omega_n &= \sqrt{\sigma^2 + w^2} = 2.88 \\ \zeta &= \frac{\sigma}{\omega_n} = \frac{0.32}{2.88} = 0.11 \end{aligned} \tag{9}$$

We can see that the poles are on the left side of the complex plane, and are hence stable with a natural frequency of $2.88 rad/sek$. This can be seen in eq. (9). The duch-roll mode will give rise to an oscillating motion in both the yaw and roll where the roll angle tilts in the negative direction around i^b while the yaw motion moves in the positive direction around k^b. If we increase the relative dampening the system will stabilize around the set point faster, with less oscillations.

Problem d

In the spiral-divergence mode we assume that $\dot{\overline{p}} = \overline{p} = 0$, which mean that the roll is fixed and stable, and that the effect of the rudder is negligible. The equation for this system is then eq. (10).

$$0 = L_v * V_a^* \cos\beta^* \overline{\beta} + L_r \overline{r} + L_{\delta_a} \overline{\delta}_a \tag{10}$$

$$\dot{\overline{r}} = N_v V_a^* \cos\beta^* \overline{\beta} + N_r \overline{\beta} + N_{\delta_a} \overline{\delta}_a \tag{11}$$

If we rearrange eq. (10) so we get $\overline{\beta}$ on one side, and substitute it for $\overline{\beta}$ in eq. (11), we get the equation eq. (12):

$$\dot{\overline{r}} = \left(N_r - \frac{N_v L_r V_a^* \cos\beta^*}{L_v V_a^* \cos\beta^*} \right) \overline{r} + \left(N_{\delta_a} - \frac{N_v L_{\delta_a} V_a^* \cos\beta^*}{L_v V_a^* \cos\beta^*} \right) \overline{\delta}_a \tag{12}$$

$$\dot{\overline{r}} = \left(\frac{N_r L_v - N_v L_r}{L_v} \right) \overline{r} + \left(\frac{N_{\delta_a} L_v - N_v L_{\delta_a}}{L_v} \right) \overline{\delta}_a \tag{13}$$

We see that the constant before $\overline{r}$ in eq. (12) and eq. (13) must be equal. We also recognise that the constant in eq. (13) is equal to the equation for the poles given in the textbook [1] on page 91. We can therefore calculate the poles for the spiral divergence as shown in .

$$\lambda_{spiral} = \left(\frac{N_r L_v - N_v L_r}{L_v} \right) = \left(N_r - \frac{N_v L_r V_a^* \cos\beta^*}{L_v V_a^* \cos\beta^*} \right) \tag{14}$$

$$\lambda_{spiral} = -0.32 - \frac{6.87 * 0.46}{-10.6} = -0.022 \tag{15}$$

This system is stable since its pole are in the negative half plane. It is nonetheless a slow system with a time constant of $\tau \approx 45.5s$.

Problem e

In the roll mode we ignore the heading state and assume that the pitch $\theta = 0$. We also assume zero sideslip, yaw rate and rudder input, $\overline{\beta} = \overline{r} = \overline{\delta}_r = 0$. This leads to the roll model eq. (16).

$$\dot{\overline{p}} = L_p \overline{p} + L_{\delta_a} \overline{\delta}_a \tag{16}$$

The eigenvalue to this system can be approximated with the eq. (17) in [1] page 90.

$$\lambda_{rolling} = L_p = -2.87 \tag{17}$$

The is shows that the roll mode is faster than the spiral-divergence mode.

Problem 2 - Autopilot for course hold using aileron and successive loop closure

The first task is to derive the transfer function from the aileron angle δ_a to the yaw-angle rate $p = \dot{\psi}$, ie. derive $h(s)$ of the form shown in equation (18).

$$h(s) = \frac{p(s)}{\delta_a(s)} = \frac{\alpha_{\phi_2}}{s + \alpha_{\phi_1}}. \tag{18}$$

The numerical values for α_{ϕ_1} and α_{ϕ_2} are found using the given state-spaced model and matrices. For roll-rate control we consider the roll mode when designing the controller. The mode is obtained by assuming that $\beta = r = 0$. This simplifies the yaw-rate model as shown in equation (**??**).

$$\begin{aligned} \dot{p} &= -10.6\beta - 2.87p + 0.46r - 0.65\delta_a \overset{\beta=0,\, r=0}{=} -2.87p - 0.65\delta_a, \\ \mathcal{L}\{\dot{p}\} &= sp(s) = -2.87p(s) - 0.65\delta_a(s) \Rightarrow \frac{p(s)}{\delta_a(s)} = \frac{-0.65}{s + 2.87}, \\ &\Rightarrow \alpha_{\phi_1} = 2.87, \quad \alpha_{\phi_2} = -0.65. \end{aligned} \tag{19}$$

Problem b)

The gains for the successive loop closure controllers are found using the procedures described in [1]. First, the proportional and derivative gains of the roll controller k_{p_ϕ} and k_{d_ϕ} are found using the maximum angle of the aileron δ_a^{max} and the design parameter e_ϕ^{max}. The values of these are given in the assignment.

$$\begin{aligned} k_{p_\phi} &\overset{(6.7)}{=} \frac{\delta_a^{max}}{e_\phi^{max}} \text{sign}(\alpha_{\phi_2}) = \frac{30^\circ}{15^\circ} \text{sign}(-0.65) \\ &= -2 \end{aligned} \tag{20}$$

Using the natural frequency of the roll loop ω_{n_ϕ} and the design parameter ζ_ϕ for the damping ratio, the derivative gain k_{d_ϕ} is found as shown in equation (21).

$$\begin{aligned} \omega_{n_\phi} &\overset{(6.8)}{=} \sqrt{|\alpha_{\phi_2}| \frac{\delta_a^{max}}{e_\phi^{max}}} = \sqrt{|-0.65| \frac{30^\circ}{15^\circ}} \approx 1.14, \\ k_{d_\phi} &\overset{(6.9)}{=} \frac{2\zeta_\phi \omega_{n_\phi} - \alpha_{\phi_1}}{\alpha_{\phi_2}} = \frac{2 \cdot 0.707 \cdot 1.14 - 2.87}{-0.65} \\ &\approx 1.94. \end{aligned} \tag{21}$$

To select a value for the roll loop integral gain k_{i_ϕ} root locus analysis is used, resulting in an interval of values for the gain within which the system remains stable. The characteristic equation expressing the closed-loop poles of the system is placed in Evans form as shown in equation (22).

$$1 + k_{i_\phi} \left(\frac{\alpha_{\phi_2}}{s(s^2 + (\alpha_{\phi_1} + \alpha_{\phi_2} k_{d_\phi})s + \alpha_{\phi_2} k_{p_\phi})} \right) = 0. \tag{22}$$

The MATLAB function rlocusplot is used to plot the poles of the system as a function of the integral gain. The gains are selected in the range $k_{i_\phi} \in [-100, 100]$. The resulting plot is shown in figure 3, where positive and negative gain values are denoted separately.

As shown in figure 3, positive gain values for k_{i_ϕ} result in a real pole on the right half-plane. Negative gain values are stable in an interval down to approximately -3.17, below which the complex conjugate poles enter the right half-plane. Therefore, a stable interval for the integral gain is approximately $k_{i_\phi} \in [-3.17, 0]$.

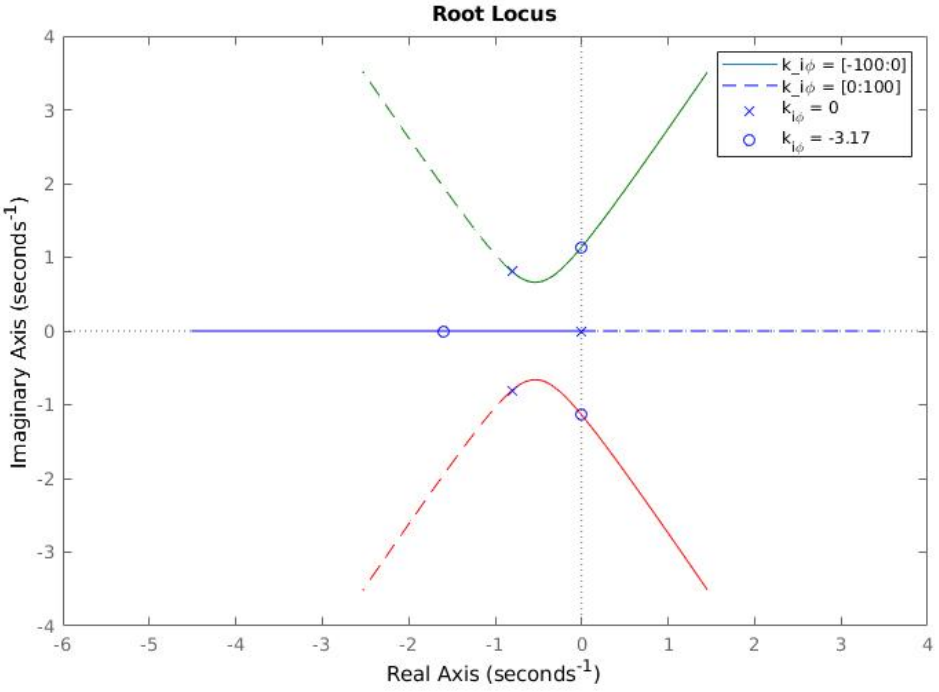

Figure 3: Roll loop root locus plot as a function of the integral gain k_{i_ϕ}

The gains for the course hold controller are tuned using the assumption that the inner loop roll gains have been adequately tuned. Following the procedure in [1], and using the design parameters χ and ζ_χ, values for the gains can be found as shown in equation (23).

$$\begin{aligned} \omega_{n_\chi} &= \frac{1}{W_\chi}\omega_{n_\phi} \approx 0.11 \quad \text{for} \quad W_\chi = 10, \\ k_{p_\chi} &\overset{(6.12)}{=} 2\zeta_\chi \omega_{n_\chi} V_g/g \approx 1.87 \quad \text{for} \quad \zeta_\chi = 0.5, \\ k_{i_\chi} &\overset{(6.13)}{=} \omega_{n_\chi}^2 V_g/g \approx 0.21. \end{aligned} \tag{23}$$

The value for W_χ is chosen to be greater than five, with good results from the choice of a value of 10. Similarly, ζ_χ is chosen to be between 0 and 1, resulting in a chosen value of 0.5.

Problem c)

As noted in [1], an integrator in the roll loop is necessary to remove the steady-state error due to disturbances that enters at the summing junction before the δ_a input to the roll-mode system. These disturbances include both the dynamics that were lost during linearization, as well as physical perturbations such as gusts or turbulence.

Adding an integrator will however have a negative phase contribution of 90, reducing stability of the system. From a practical viewpoint, there is no bias term in the internal loop which would result in a steady-state error. Therefore, the integral term can be removed, as is done for the remeainder of the assignment.

Simulation results with and without the integral action shows that it has a negative effect on stability for course angle reference changes of more than around 15°, as shown in figure 4.

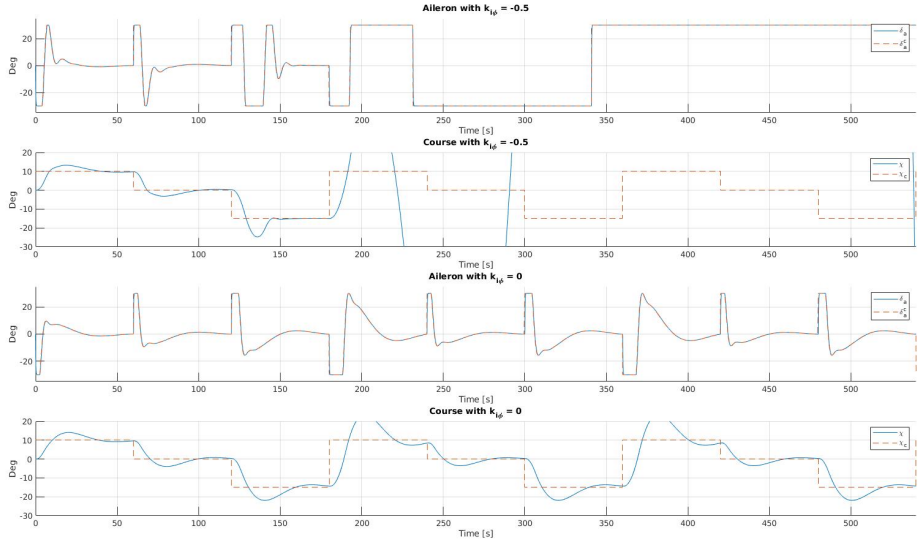

Figure 4: Simulation results of course angle following with and without integral control on the roll loop.

Problem d)

The course following simulation is run for 540 seconds, with a repeating step reference of sequence $\chi_c = [10°, 0°, -15°]$, where the reference switches every 60 seconds. This results in reference changes of 10°, 15° and 25°. The resulting course angle χ and aileron angle δ_a are plotted in figure 5.

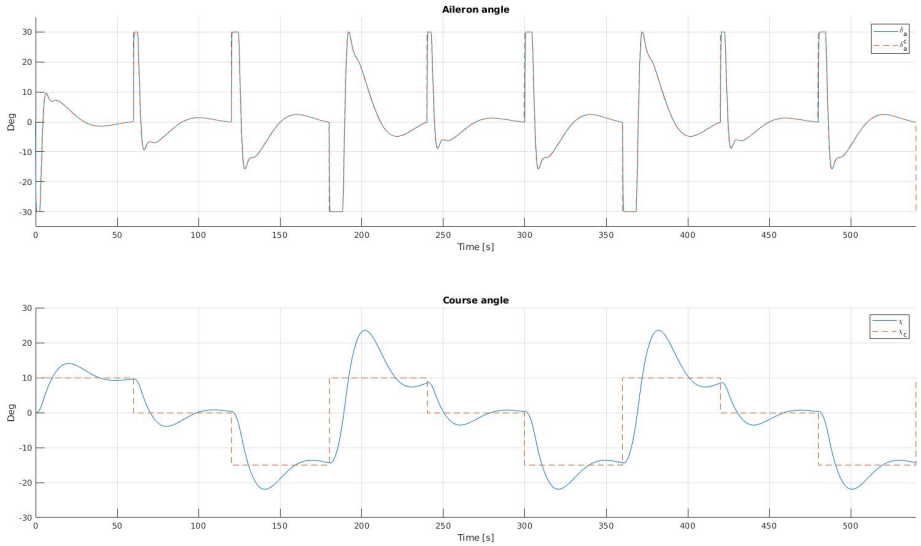

Figure 5: Simulation results of course angle following.

Problem e)

In this section the system is simulated with the complete state-space model. The main objective is to analyze how well the linearized and simplified model from the previous section performs

compared to the full system. The simulated full state model is shown in fig. 6. In the complete system, the actuator dynamics and the real coordinated turn equation are included as well. The control gains are kept the same from previous sections.

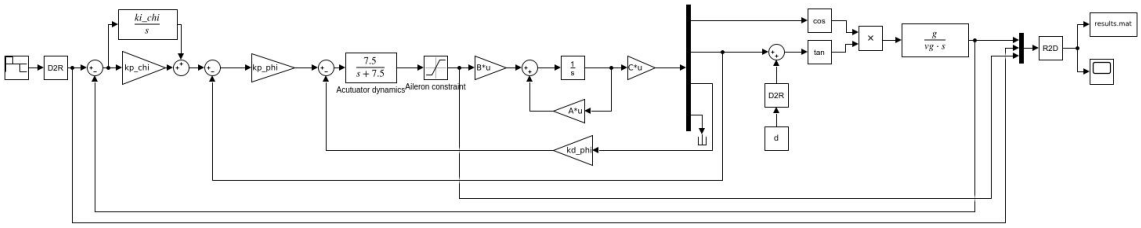

Figure 6: Block diagram of full state-space model in Simulink

The system is simulated with two different sets of course changing maneuvers, first with increments of 2° and then with 10° increments as shown in fig. 7. This is done to observe how well the linearized system performs for small and large course changing maneuvers. As expected, the linearized and simplified model accurately reproduces the full system response for small course angle inputs (i.e $\chi = \pm 2°$), and this deviates as input gets larger and larger (i.e $\chi = \pm 10°$). This is due to the simplification of $\tan\phi \approx \phi$ for small ϕ in the coordinated turn equation.

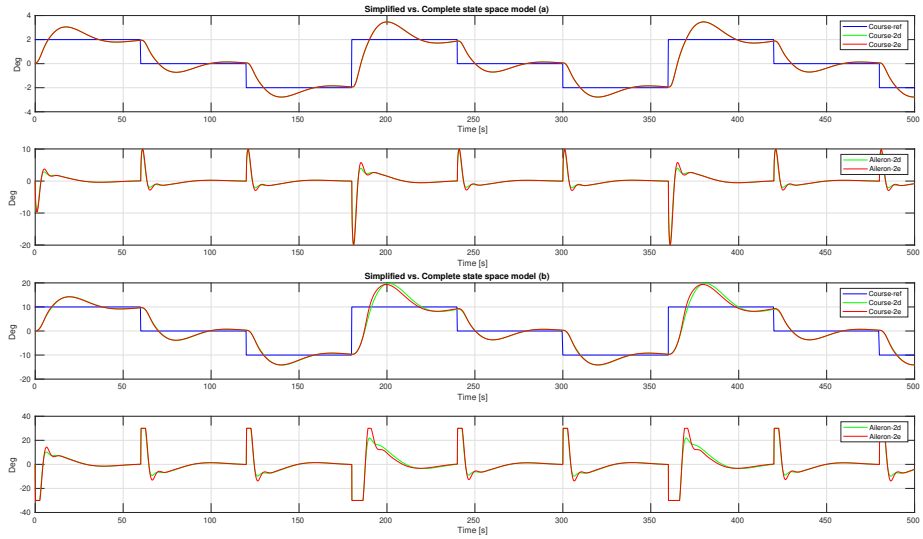

Figure 7: (a)-The aileron input δ_a and course angle $\chi = \pm 2°$ for the linearized system (green) and full state space model (red). (b)-The aileron input δ_a and course angle $\chi = \pm 10°$ for the linearized system (green) and full state space model (red).

The system becomes unstable when the course reference is pushed to values higher than the recommended limits provided in the exercise ($|\chi_{max}| = 15°$). This constraint is valid as it is not expected by a system to perform well provided saturation constraints and delay-dynamics on the actuator system. Both system simulated with course jumps of 30° leads to unstable response due to aileron actuator saturation as shown in fig. 8.

Problem f)

In the previous task we saw that the control input saturated at $\delta_a = 30\,\text{deg}$ for a long period of time. Noticing that the aileron angle δ_a stays saturated for approximately 10 seconds in the first step response, gives the integrator a lot of time to build up error, and hence integrator windup becomes a problem. The error becomes unreasonable big as the windup continues, and when the

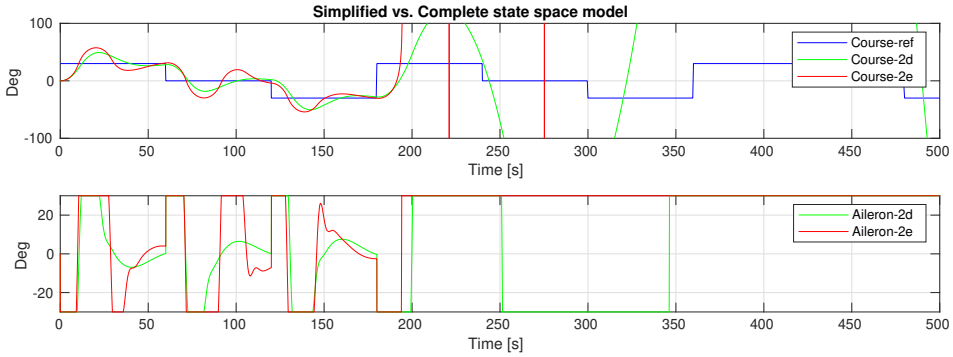

Figure 8: The aileron input δ_a and course angle $\chi = \pm 30°$ for the linearized system (green) and full state space model (red).

saturation ends the integrator needs time to adjust the error accordingly, and hence can make a system unstable. Integrator windup is a problem in any situation where the control inputs saturates and should be treated.

A solution to the integrator windup, is to stop the integration of error when a saturation of the input is detected. In this case, the integration of course error is stopped when the aileron angle δ_a saturates at ± 30 deg. The integration continues when the saturation ends.

In fig. 9, the logic on stopping the integrator windup is implemented. From the plots we can see that the controllers successfully controls the course χ to the desired course χ_c within 60 seconds for each change in maneuvers. The reference starts at 15 deg, then shifts to 0 deg at 60 seconds and then changes again at 120 seconds to -15 deg.

From the figure we can compare the dynamics with and without the anti-windup configuration. With the anti-windup logic implemented, the input stays saturated for a shorter period of time and has lower amplitudes in the oscillatory modes. The course angle also has lower amplitudes in the oscillatory modes. Thus, the anti-windup logic has further improved our system.

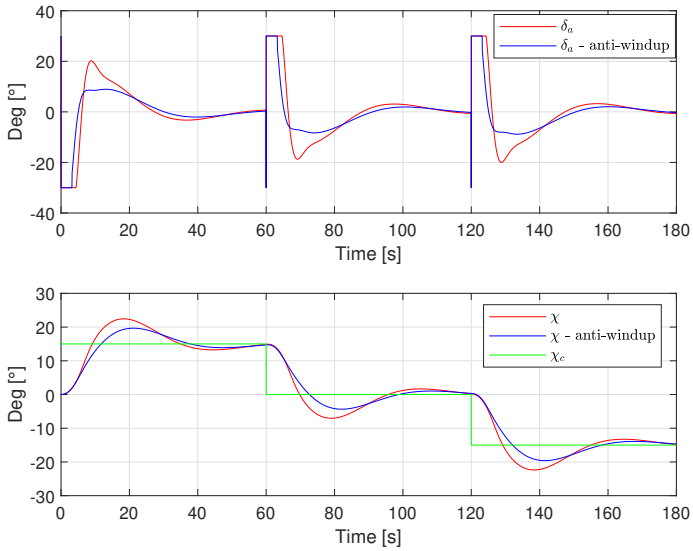

Figure 9: The aileron input δ_a and course angle χ with(blue) and without(red) anti-windup logic.

References

[1] R. Beard and T. McLain, "Small unmanned aircraft: Theory and practice," *Small Unmanned Aircraft: Theory and Practice*, 02 2012.